JACS
JOURNAL OF THE AMERICAN CHEMICAL SOCIETY
Article
pubs.acs.org/JACS

5-Azido-2-aminopyridine, a New Nitrene/Nitrenium Ion Photoaffinity Labeling Agent That Exhibits Reversible Intersystem Crossing between Singlet and Triplet Nitrenes

Maxim S. Panov, Valentyna D. Voskresenska, Mikhail N. Ryazantsev,† Alexander N. Tarnovsky,* and R. Marshall Wilson*

Department of Chemistry and Center for Photochemical Sciences, Bowling Green State University, Bowling Green, Ohio 43403, United States

Supporting Information

ABSTRACT: The photochemistry of a new photoaffinity labeling (PAL) agent, 5-azido-2-(*N*,*N*-diethylamino)pyridine, was studied in aprotic and protic solvents using femtosecond-to-microsecond transient absorption and product analysis, in conjunction with *ab initio* multiconfigurational and multireference quantum chemical calculations. The excited singlet S_1 state is spectroscopically dark, whereas photoexcitation to higher-lying singlet excited S_2 and S_3 states drives the photochemical reaction toward a barrierless ultrafast relaxation path via two conical intersections to S_1, where N_2 elimination leads to the formation of the closed-shell singlet nitrene. The singlet nitrene undergoes intersystem crossing (ISC) to the triplet nitrene in aprotic and protic solvents as well as protonation to form the nitrenium ion. The ISC rate constants in aprotic solvents increase with solvent polarity, displaying a "direct" gap effect, whereas an "inverse" gap effect is observed in protic solvents. Transient absorption actinometry experiments suggest that a solvent-dependent fraction from 20% to 50% of nitrenium ions is generated on a time scale of a few tens of picoseconds. The closed-shell singlet and triplet nitrene are separated by a small energy gap in protic solvents. As a result, the unreactive triplet state nitrene undergoes delayed, thermally activated reverse ISC to reform the reactive closed-shell singlet nitrene, which subsequently protonates, forming the remaining fraction of nitrenium ions. The product studies demonstrate that the resulting nitrenium ion stabilized by the electron-donating 4-amino group yields the final cross-linked product with high, almost quantitative efficiency. The enhanced PAL function of this new azide with respect to the widely applied 4-amino-3-nitrophenyl azide is discussed.

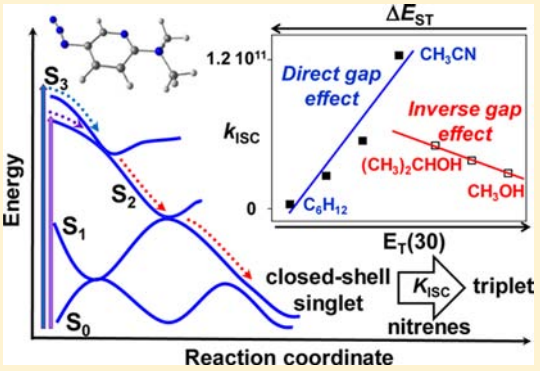

INTRODUCTION

Photoaffinity labeling and photocross-linking (PAL/PCL) continues to evolve as a major technique for studying molecular interactions in biological systems.[1−7] In this method, the PAL agent specifically and reversibly binds to the active site of the biomolecule where irradiation generates an extremely reactive intermediate that is thought to rapidly and irreversibly react with the target site before they can drift apart. Great progress in the development of new PAL agents and understanding of the photoaffinity labeling processes has been made over the past ten years. It is of critical important to determine the photochemical mechanisms of these PAL agents in considerable detail so as to aid in the design of more effective agents and increase their labeling selectivity and efficiency.

The PAL agent, 4-fluoro-3-nitrophenyl azide, is a system that has been widely applied in photoaffinity studies with different classes of biological molecules in recent years.[8−13] Recently, we have studied the photochemical mechanism of its amine analogue, 4-amino-3-nitrophenyl azide (**1**), in the presence of nucleophiles using ultrafast transient absoprtion and quantum chemical computational techniques.[14] This molecule is promoted to its first excited singlet S_1-state (π, π^*) by absorption of a 420-nm photon and undergoes unproductive fast internal conversion to the vibrational manifold of the ground electronic state on a ∼350-fs time scale. On the other hand, 350-nm excitation of **1** to its second excited singlet S_2-state (π, π^*) leads to two reaction pathways: the recovery of the electronic ground state of the parent molecule and N_2 elimination (Scheme 1). Excitation at 305 nm favors this

Scheme 1

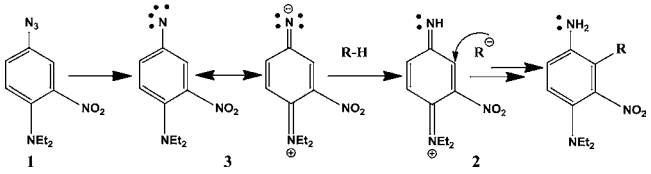

Received: June 14, 2013
Published: November 12, 2013

dx.doi.org/10.1021/ja405637b | J. Am. Chem. Soc. 2013, 135, 19167−19179

second nitrogen-elimination channel, but some internal conversion back to the ground state still takes place. The presence of the nitro group as a strong electron-withdrawing substituent on the benzene ring has a dramatic effect on the reactivity of the diiminoquinone nitrenium ion intermediate **2** produced in this photolysis. The generation of the nitrene **3** from **1** occurs on the S_2 surface, and this reaction intermediate is a powerful base that abstracts protons extremely rapidly from a variety of sources to form diiminoquinone nitrenium ion **2**. This nitrenium ion, augmented by the nitro group, becomes a powerful electrophile and reacts with the conjugate base of the acid that led to its formation. The protonation of the nitrene by methanol observed in this work ranks with the fastest intermolecular proton transfer processes known, which include the protonation of singlet diphenylcarbene by methanol, τ = 9 ps,[15] and the protonation of water by several excited photoacids.[16]

However, **1** has several disadvantages: the nitro group is bulky, so reactions with some target molecules are sterically hindered, and in addition the nitro group is photoreactive itself. With these considerations in mind, we set out to design and synthesize a new azide that might be used as a more effective photoaffinity-labeling agent than the nitro analogue **1**. The 5-azido-2-aminopyridine (**4**) was selected as a possibly improved PAL reagent (Figure 1). Nitrogen-containing heterocyclic

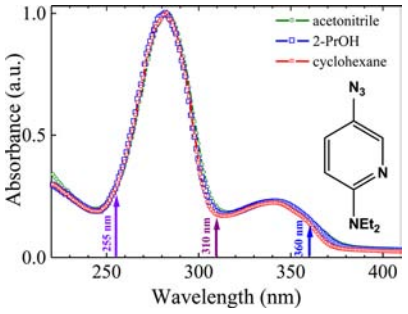

Figure 1. UV−vis absorption spectra of **4** in several solvents normalized to unity at the absorption maximum. The arrows indicate the excitation wavelengths used in the current study.

compounds with azido groups have attracted considerable attention as photoaffinity labeling reagents.[17−20] Common photochemistry of pyridyl azides includes photochemical ring expansion leading to seven-membered di-*N*-heterocyclic ring via the singlet nitrenes and generally is thought to be very similar to the photochemistry of other aryl azides.[17,18,21,22] However, just as with the azide **1**, the introduction of the amino substituent *para* to the azide in **4** suppresses the ring-expansion mode and favors formation of nitrenium ion.

In this work, the photochemical mechanism of the azide **4** and possible advantages of this modified system are investigated using product analysis, time-resolved (from 100 fs to several microseconds) transient absorption, and *ab initio* quantum chemical calculations. The photocross-linking chemistry of **4** is shown to proceed through a previously unrecognized mechanism in which the highly reactive closed-shell singlet nitrene **6** and the unreactive triplet nitrene **7** are in equilibrium with each other and proceed with nearly quantitative efficiency cross-linked products. Thus, reaction of the reactive nitrene **6** is bimodal. This species is formed rapidly in the femtosecond time domain and either forms the nitrenium ion **5** or undergoes ISC to the triplet nitrene **7** in the picosecond time domain. This ISC process is both environment-dependent, following the direct "gap" effect[23−27] in aprotic solvents and the "inverse gap" effect[23−27] in protic solvents, and reversible. The reversibility of the ISC greatly extends the effective lifetime of the closed-shell singlet nitrene and in many ways is analogous to the mechanism of thermally activated delayed fluorescence.[28]

METHODOLOGY

Synthetic Procedures and Sample Characterization. All experiments were performed on the azide **4** at 22 °C. Solvents used (methanol, ethanol, 2-propanol, *n*-butanol, *tert*-butanol, toluene, methyl acetate, acetonitrile, and cyclohexane) were purchased from Aldrich or EMD Chemicals. Imidazole hydrochloride was purchased from Aldrich. Methyl acetate, toluene, and acetonitrile were used in anhydrous form.

Ultrafast Transient Absorption. The setup described previously[14] is based on an amplified Ti:sapphire laser system (90 fs, 800 nm, and 1 kHz). Transient absorption (ΔA) spectra of **4** were recorded at excitation wavelengths of 360, 310, and 255 nm produced by a TOPAS-C optical parametric amplifier. Femtosecond pulses tunable from 280 to 390 nm from another TOPAS-C or a white-light continuum from 340 to 720 nm were used as probe light. The instrument response function (150 fs, fwhm) was measured using a Gaussian-like ΔA signal at time zero due to stimulated Raman scattering from neat solvent.[29] All ΔA spectra of **4** were measured at magic angle polarization conditions and corrected for the group velocity dispersion of the probe light with an accuracy of 30 fs by using cross-phase modulation or two-photon (pump plus probe) absorption signals from neat solvent.[30,31] Multiexponential fits of ΔA kinetic traces and decay-associated global fits[32] of ΔA spectra were employed to characterize the temporal evolution of the reactive species. The solvent signals[30,31] persist for 100−200 fs after excitation, so this region (300 fs upon 255-nm excitation) was excluded from fitting. The ΔA kinetic traces as a function of delay time (t) were fitted to a sum of exponential functions: $\Delta A = \Delta A_0 + \sum_i A_i\, e^{-t/\tau_i}$, where τ_i are the time constants, A_i are the amplitudes, ΔA_0 is the permanent spectrum at infinitely long times ($\gg$1 ns). The ΔA spectra were globally fitted to a sum of exponentials $\sum_j \varepsilon_j(\lambda)\, \exp(-t/\tau_{j,g})$, where $\tau_{j,g}$ are the time constants, and $\varepsilon_j(\lambda)$ are the decay-associated spectra characteristic of the $\tau_{j,g}$ time components and reconstructed from these values based on the assumption of a consecutive reaction mechanism.

Microsecond Transient Absorption. The ΔA spectra were collected using a Proteus spectrometer[33] equipped with a 150 W Xe arc lamp, a monochromator, and photodiode detectors. Excitation 355-nm pulses of ∼10-ns width with energy of 3−5 mJ from a Nd:YAG laser/OPO system (10 Hz) were directed to the sample with an absorbance of 0.6−0.8 at 355 nm.

Computational Details. All calculations were performed for the azide **4**, where Et was replaced by Me to minimize the computational cost, and its products (closed-shell singlet nitrene **6**, open-shell singlet nitrene **8**, triplet nitrene **7**, nitrenium ion **5**, adduct/product **9**/**10**) using Gaussian 03[34] and MOLCAS 7.4.[35] The geometries of **4** and **6**−**10** were optimized using MP2/cc-pVDZ,[36] where solvent effects were accounted by the conductor-like polarizable continuum model (CPCM).[37] Also, the complete active space self-consistent field (CASSCF) methodology was used to optimize the **4**−**10** geometries at CASSCF/6-31G* CPCM.[38] The conical intersection seams (CIs) were optimized at CASSCF(12,10)/6-31G*, whereas the Moplot graphical program[39] was employed to visualize the lower cone of optimized CIs. Minimum energy paths (MEPs) were computed using the intrinsic reaction coordinate method (IRC)[40] at CASSCF(14,12)/6-31G*. Using the complete active space second order perturbation theory (CASPT2),[41] vertical excitation transition (VET), and oscillator strength (f) calculations were performed at the optimized geometries utilizing the CASPT2//CASSCF protocol and the scalar relativistic atomic natural orbital basis set (ANO-RCC).[42]

dx.doi.org/10.1021/ja405637b | J. Am. Chem. Soc. 2013, 135, 19167−19179

SYNTHESIS AND PRODUCT ANALYSIS

The route used to synthesize **4** is shown in Scheme 2. Irradiation of the solutions of **4** under a nitrogen atmosphere

Scheme 2

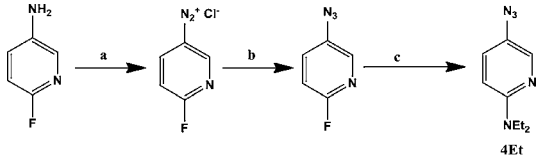

a) HCl, $NaNO_2$, -15°C; b) NaN_3, H_2O, $NaHCO_3$, 0°C; c) DEA, EtOH, 45°C

was conducted in a Pyrex tube at 350 nm in a Rayonet photochemical reactor at 20−25 °C. The photolysis of **4**, performed in the presence of alcohols (HOR), leads to the formation of addition products **10** (Nuc = OR) in excellent yields (Table 1 and Scheme 3). The irradiation of **4** in 2-PrOH

Table 1. Reduction/Addition Yields for Photoreactions of 4 with Various Nucleophiles

	products ratio		
nucleophiles	reduction (**12**)	substitution (**10**)	time of irradiation (h)
MeOH	20	80	2.5
2-PrOH	0	100	2.5
2-PrOD	2	98	0.5
n-BuOH	0	100	0.7
t-BuOH	0	100	3.5
C_6H_5OH	0	100	3.0
imidazole HCl	0	100	4.0
$(CH_3)_2NH$ HCl	2	98	3.0

Scheme 3

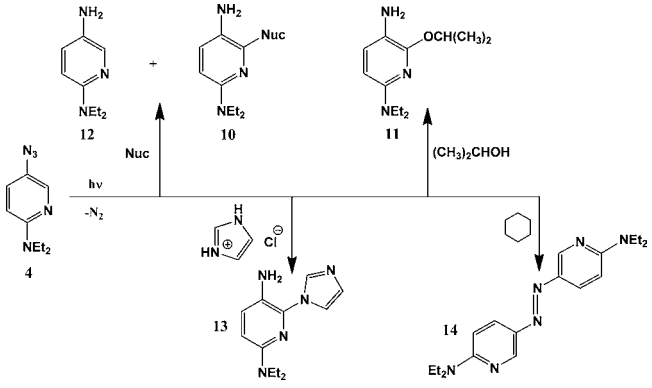

leads to the formation of only one addition product **11** (the 2-substituted adduct); the 4- or 5-substituted products were not observed. The addition process with **4** proceeds much more effectively, in a range from 80% to 100%, in comparison to the nitro analogue **1**. Moreover, in **4** the conversion of starting material to product was more rapid and proceeds to completion in 0.5−4 h. Experiments in saturated solutions of phenol and dimethylammonium salt in acetonitrile provided complete conversion to ratios of **10**/**12** = 100/0 and 98/2, respectively (Table 1). Furthermore, irradiation of **4** in *tert*-butanol leads to complete conversion of starting material to the addition product **10**, Nuc = *t*OBu. Photolysis with imidazole hydrochloride in acetonitrile led exclusively to the corresponding adduct **13** (Scheme 3). It is noteworthy that no substitution reaction occurred in the presence of imidazole in acetonitrile. Photolysis of **4** in cyclohexane was completed within 3 h and afforded a single product: the dimer **14**, which suggests the intermediacy of triplet nitrene in this nonprotonating solvent. The aniline reduction product **12** and the dimer **14** in ratio 3:1 were obtained upon photolysis of **4** in toluene.

COMPUTATIONAL RESULTS

Photochemical Reaction Paths. The CASPT2//CASSCF(16,13)/ANO-RCC VETs of **4** from the ground state (S_0) to the three low-lying excited singlet states (S_1, S_2, and S_3) show that the lowest energy transition $S_0 \rightarrow S_1$ has a small oscillator strength, f = 0.0002. In contrast, the $S_0 \rightarrow S_2$ transition at λ_{max} = 314 nm (f = 0.0274) and the $S_0 \rightarrow S_3$ transition at λ_{max} = 260 nm (f = 0.1999) are both intense. The S_1, S_2, and S_3 states are all (π, π^*).

The CASSCF photochemical reaction paths following excitation of **4** into S_1, S_2, and S_3 were obtained to determine which one is responsible for N_2 extrusion. Following vertical excitation of **4** into the S_1 state, the MEP starting from the Franck−Condon (FC) point reveals an S_1/S_0 conical intersection (CI) (Figure 2). The MEP restarted from the vicinity of the CI leads to the formation of ground-state **4** or photoproducts (nitrene and molecular nitrogen). This nitrene has two singly occupied molecular orbitals, the 2p-π (5) and in-plane 2p orbital (12) on N, and therefore is identified as the open-shell singlet (**8**) species (see Supporting Information for orbital numbering). Following vertical excitation of **4** into S_2, the S_2 and S_1 potential energy surfaces approach each other along the MEP; however, the intersection point is not reached within the scan. The MEP starting from the S_3 FC region locates the S_3/S_2 CI and then proceeds to the CI(S_2/S_1), Figure 3. From the S_2/S_1 CI, the relaxation process on the S_1 surface leads to the formation of the nitrene and N_2. This nitrene exhibits a closed-shell electronic configuration with the empty in-plane p-orbital (**9**) on a nitrogen atom and the doubly occupied the 2p-π orbital (7), corresponding to the unrelaxed closed-shell singlet nitrene geometry, which after optimization yields the relaxed geometry of this species where the orbital occupancies are reversed (nitrene **6**) (Figure 4). The active space orbital occupancies and the Moplot[39] topologies are given in Supporting Information.

Product Geometries and Energetics. Figure 4 shows the CASSCF molecular orbitals included in the active space of the triplet nitrene **7**, open-shell singlet nitrene **8**, and closed-shell singlet nitrene **6**. Figure 5 shows the optimized geometries of these species. The pyridine moieties in the optimized geometries of **7** and **6** are very similar. The CASSCF(10,8)/6-31G* level of theory predicts that **8** is 21 kcal mol^{-1} and **6** is 33 kcal mol^{-1} higher in energy than **7** in vacuum. However, the energy gap between **6** and **7** becomes much smaller in polar solvents such as methanol (5.5 kcal mol^{-1}). In contrast, for the azide **1** the CASSCF(10,8)/6-31G* calculations predict much larger energy difference between the triplet and the closed-shell singlet nitrenes in the gas phase and methanol, 40 and 36 kcal mol^{-1}, respectively (Supporting Information). The above trend is supported by electric dipole moments of the involved species. Electric dipole moments of the triplet and the closed-shell singlet nitrenes derived from **1** and **4** are calculated to be 6.1 and 6.9 D and 4.1 and 7.8 D, respectively. A larger dipole moment is typically correlated with a stronger dependence of the corresponding electronic state energy on medium polarity.

dx.doi.org/10.1021/ja405637b | J. Am. Chem. Soc. 2013, 135, 19167−19179

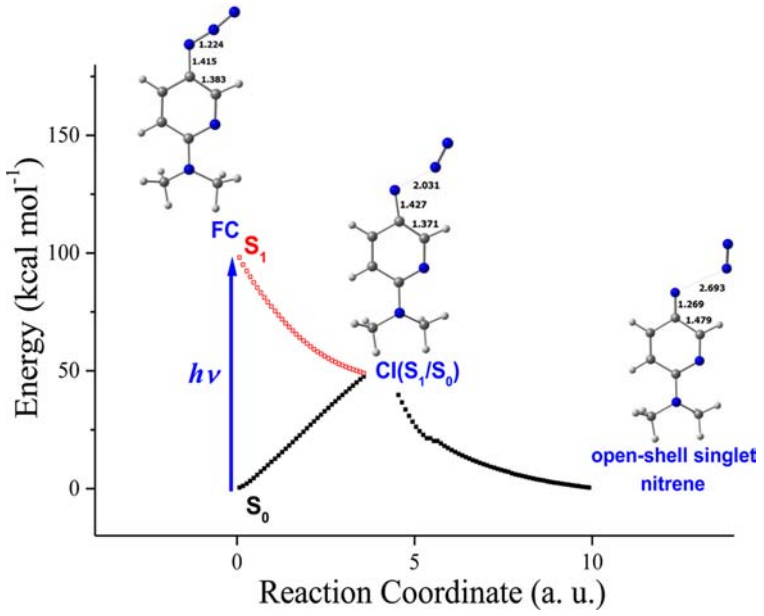

Figure 2. CASSCF MEPs starting from the S_1 Franck–Condon point (FC) of **4** to the S_1/S_0 conical intersection (CI) and from the CI toward the formation of the photoproducts.

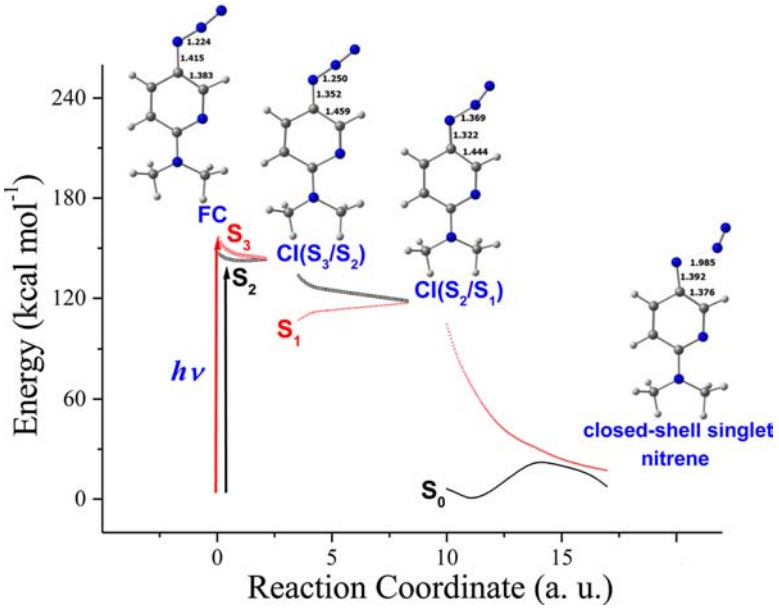

Figure 3. CASSCF MEPs from the S_3 FC point of **4** toward the formation of the photoproducts via the S_3/S_2 and S_2/S_1 CIs.

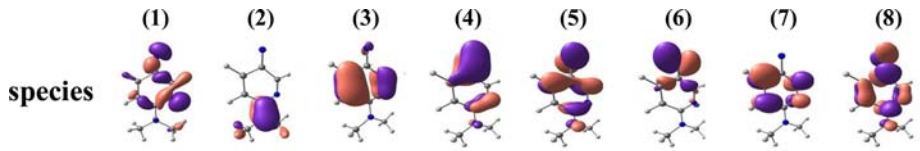

Figure 4. Occupancy of the molecular orbitals of the nitrenes derived from **4** upon completing their geometry optimization at the CASSCF(10,8)/6-31G* level of theory.

Indeed, **4** is substituted with a powerful electron-donating amino group, which should stabilize the closed-shell singlet nitrene with respect to other product states due to π-electron donation to the empty p-orbital on N. Consequently, **6** is more polar than **7**, and their energy gap is expected to decrease with increasing solvent polarity, in agreement with the calculations. The CASPT2 VETs for **6**–**8** and several other reactive species derived from irradiation of **4** are shown in Table 2.

dx.doi.org/10.1021/ja405637b | J. Am. Chem. Soc. 2013, 135, 19167–19179

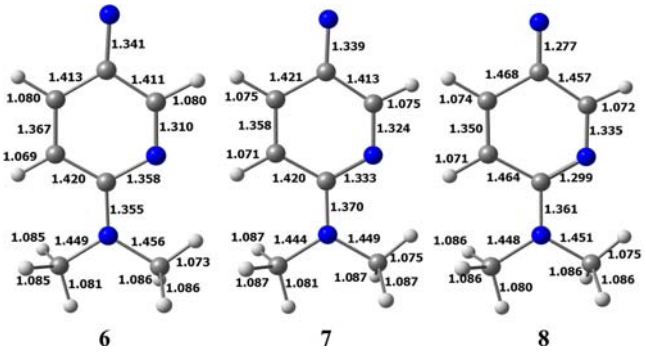

Figure 5. Optimized geometries of the closed-shell singlet **6** singlet, the triplet **7**, and the open-shell singlet **8** nitrenes computed using CASSCF(10,8)/6-31G* CPCM in methanol.

Table 2. CASPT2//CASSCF/ANO-RCC Vertical Excitation Transitions and Oscillator Strengths of Possible Reactive Species Derived upon Irradiation of 4

species	λ (nm) (f, oscillator strength)	λ (nm) experiment[a]
closed-shell singlet nitrene **6**	807 (0.0100)	328
	601 (0.0192)	
	437 (0.0110)	
	350 (0.1220)	
	340 (0.2110)	
	308 (0.4920)	
open-shell singlet nitrene **8**	479 (0.0073)	–
	346 (0.0749)	
	337 (0.0074)	
	278 (0.0030)	
triplet nitrene **7**	422 (0.0240)	456
	418 (0.0236)	435
	271 (0.0293)	312
nirenium ion **5**	490 (0.0079)	500–550
	290 (0.0950)	
adduct **9**	288 (0.0297)	380–410
product **10**	301 (0.4945)	250–330

[a]The absorption maxima of these species compiled from steady-state and time-resolved spectroscopy data obtained throughout this work are presented for comparison.

SPECTROSCOPIC RESULTS

Steady-State Absorption. The UV–vis absorption spectrum of **4** in 2-PrOH consists of two broad bands: a weak band is located at 340 nm (ε = 5969 M^{-1} cm^{-1}), and a stronger one is centered at about 280 nm (ε = 18690 M^{-1} cm^{-1}) (Figure 1). The UV–vis spectra of **4** exhibit no solvatochromic shift. It should be noted that solutions of **4** do not exhibit any noticeable fluorescence upon irradiation in the 280–360 nm range.

Ultrafast Transient Absorption. In neat cyclohexane upon 360-nm excitation, any significant ΔA signals occur at delay times between −50 and 50 fs. Following 360-nm excitation of **4** in cyclohexane, the 100-fs ΔA spectrum consists of a 330-nm UV band and a broad visible band with a maximum at ∼485 nm (Figure 6A). Between 1 and 20 ps, transient absorption narrows, blue-shifts, and decays (Figure 6B). From 50 ps to several hundreds of picoseconds, the 313- and 456-nm product absorption bands grow and the 350-nm ground-state bleach signal becomes pronounced, indicating that

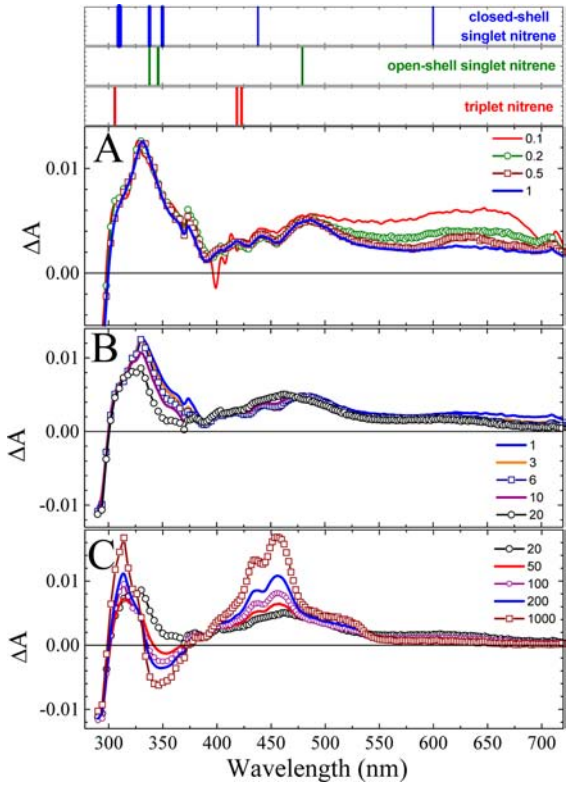

Figure 6. ΔA spectra of a 0.25-mm flowing jet of **4** (1.3 mM) in cyclohexane excited at 360 nm (pulse energy, 4.1 μJ). Delay times between the probe and pump pulses (in picoseconds) are shown in the legends. Top panels show the allowed CASPT2 vertical excitation energies of **6**, **7**, and **8** where bar thickness is proportional to the calculated oscillator strengths.

the overlapping 330-nm band decays (Figure 6C). The 1000-ps ΔA spectrum displays the 313-nm band as well as the visible 456-nm band with two shoulders at 436 nm and ∼510–515 nm. The 330- and 485-nm transients agree with the CASPT2 VETs calculated for the singlet closed-shell nitrene **6**. The 313-, 436-, and 456-nm ΔA bands at long times are consistent with the CASPT2 VETs predicted for the triplet nitrene **7** (Figure 6).

The 100- and 200-fs ΔA spectra of **4** in 2-PrOH following 360-nm excitation display an intense ∼322-nm band and a broad ∼475-nm band, Figure 7. From 1 to 50 ps, the 322-nm band and the red ΔA absorption decay concurrently with a rise of the 314-nm band of **7** and the visible 475-nm band, which (albeit with a minor decay) remain to 1000 ps (Figure 7C). The ΔA spectral evolution of **4** upon 310-nm excitation (Supporting Information) and 255-nm excitation (Figure 7D–F) is rather similar. However, the 300-fs UV ΔA band is much broader upon 255-nm excitation compared to that at 360 nm, suggesting that the species responsible for the short-time UV band is produced with an excess of vibrational energy. This nascent species is assigned to **6**, consistent with the CASPT2 VET calculations.

The ΔA spectra were also measured following 360-nm excitation of **4** in methanol (Figure 8) and several other solvents (Supporting Information). The ΔA spectra were also measured for **4** in a mixture of acetonitrile and imidazole hydrochloride (Supporting Information). Imidazole mimics the amino acid histidine and, therefore, is a good model for studies of **4** as a potential PCL/PAL system. Spectral profiles of the

dx.doi.org/10.1021/ja405637b | J. Am. Chem. Soc. 2013, 135, 19167–19179

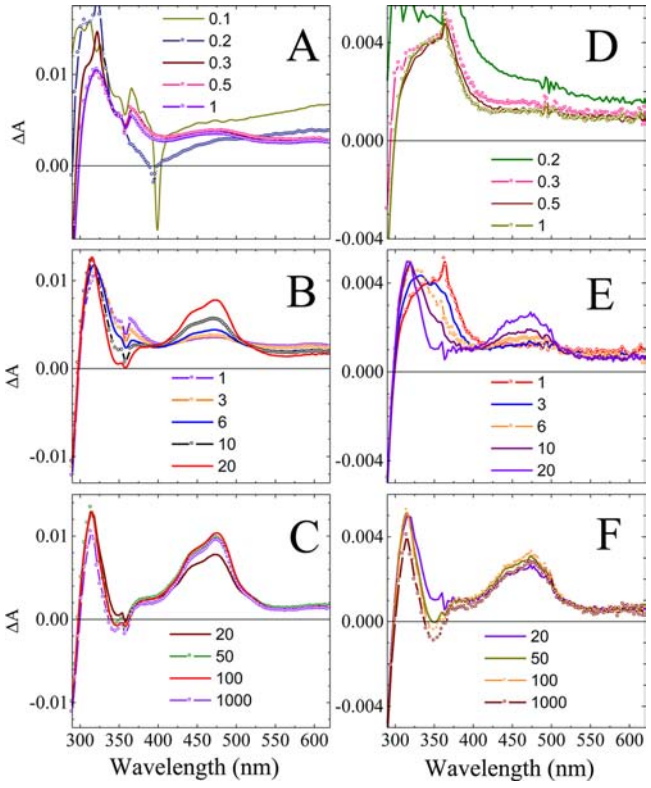

Figure 7. ΔA spectra of **4** (1.1 mM, 0.2-mm flow cell) in 2-PrOH for various delay times (in picoseconds, shown in the legends). Solutions were excited either at 360 nm (A–C) or 255 nm (D–F) with an energy of 6.1 μJ pulse^{-1}. The ΔA signals for λ > 525 nm (0.1 ps) are due to solvent cross-phase modulation and impulsive stimulated Raman scattering, and those from 395 to 405 nm ($\lesssim$0.2 ps) are due to solvent stimulated Raman scattering.

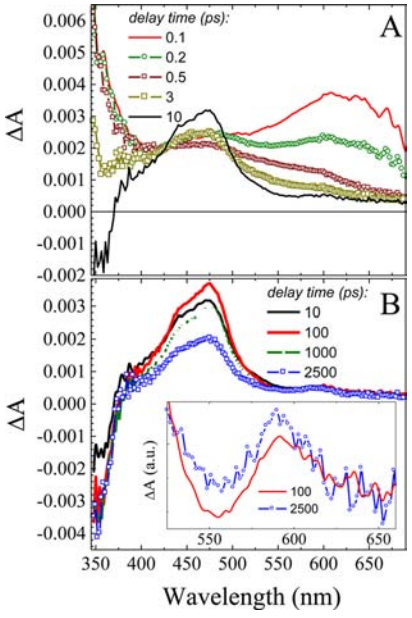

Figure 8. ΔA spectra of **4** (1.1 mM, 0.2-mm flow cell) in MeOH excited at 360 nm (0.8 μJ pulse^{-1}). The inset shows the 100- and 2500-ps ΔA spectra normalized at the long-wavelength wing.

visible product ΔA bands in several selected solvents are compared in Figure 9. For **4** in protic solvents, the spectral evolution of transient absorption resembles that observed in 2-

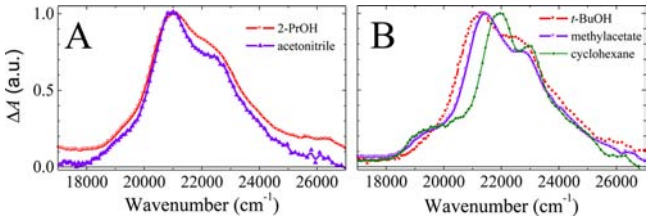

Figure 9. Visible product bands (normalized to unity) from the 1-ns ΔA spectra of **4** measured in protic and aprotic solvents of similar polarity. (A) 2-PrOH and CH_3CN, $E_T(30)$ = 48.4 and 45.6, respectively. (B) *t*-BuOH and $C_3H_6O_2$, $E_T(30)$ = 43.3 and 38.9, respectively. Nonpolar C_6H_{12} ($E_T(30)$ = 34.3) is added for comparison.

PrOH. The 470–475-nm band forms on a time scale of ten to several tens of picoseconds, being the fastest in CH_3OH and slowest in butanols. With decreasing solvent polarity, this visible band exhibits a minor hypsochromic shift. The 470–475-nm band decays faster in the alcohols with shorter carbon chain lengths. In methanol solutions investigated to a 2.5-ns delay time, the decay of this band is accompanied by a rise of transient absorption in the 530–580 nm range, Figure 8B, inset. In 2-PrOH, the aforementioned rise occurs to a much lesser degree. In the aprotic solvents and acetonitrile/imidazole hydrochloride mixture (Supporting Information), the ΔA spectral evolution resembles that observed in cyclohexane, albeit occurring much faster. The visible absorption band exhibits no noticeable decay within 1 ns, except for the aforementioned mixture where some decay is observed similar to that in *t*-BuOH.

Fitting Analysis. The best-fit parameters of multiexponential fits (component time constants, τ_1 and τ_2) of ΔA kinetic traces performed at wavelengths characteristic of the temporal evolution of the transient species are summarized in Supporting Information. These two components are dominant in all solvents investigated, describing the short-time spectral reshaping (τ_1) and the formation of the 470–475 bands as well as the decay of the UV and red absorption (τ_2). In 2-PrOH, τ_2 = 16 ps, independent of the excitation wavelengths. In protic solvents, τ_2 values range from 10.5 ps in CH_3OH to 19.5 ps in *t*-BuOH, generally becoming larger with increasing carbon chain length of the solvent molecule. Under the assumption that the visible bands single-exponentially relax to zero, the following decay time constants can be deduced (in ns): 4.2 (MeOH), 6.5 (EtOH), 18 (2-PrOH), 12.5 (*n*-BuOH), and 13.7 (*t*-BuOH). In aprotic solvents, τ_2 changes from 8.1 ps in acetonitrile to 38 ps in less polar toluene. Cyclohexane is unique in the sense that τ_1 and τ_2 are significantly larger compared to the other solvents investigated: τ_1 = 22 ps and τ_2 = 280 ps (Supporting Information).

A satisfactorily global fit to the ~350–620 nm ΔA spectra in all solvents requires a sum of two decay-associated spectra (ε_i) obeying exponential time dependences (time constants $\tau_{1,g}$ and $\tau_{2,g}$, Table 3) and a permanent spectrum; see Figure 10 for **4** in 2-PrOH and cyclohexane. The $\tau_{1,g}$ represents spectral narrowing and the $\tau_{2,g}$ describes the ~450 nm product absorption rise. The $\tau_{1,g}$ and $\tau_{2,g}$ values agree with the τ_1 and τ_2, indicating the consistency between these two fitting procedures.

Transient Absorption Actinometry. The formation of the nitrenium ion **5** and triplet nitrene **7** products was quantified in MeOH, 2-PrOH, *n*-BuOH, CH_3CN, and C_6H_{12}

dx.doi.org/10.1021/ja405637b | J. Am. Chem. Soc. 2013, 135, 19167–19179

Table 3. Transient Cascade Characteristics upon Excitation of 4 in Various Solvents

	solvent	pump λ (nm)	λ_{max} (nm), ε_1	$\tau_{1,g}$ (ps)	λ_{max} (nm), ε_2	$\tau_{2,g}$ (ps)	λ_{max} (nm), ε_3
1	CH_3OH	360	470	1.7	478	7.3	480
2	C_2H_5OH	360	481	1	453	8	471
3	$(CH_3)_2CHOH$	255	488	2.2	464	15	476
4	$(CH_3)_2CHOH$	310	485	2.3	458	16	471
5	$(CH_3)_2CHOH$	360	487	1.7	464	16	478
6	*n*-C_4H_9OH	360	479	2.3	450	17	471
7	*t*-C_4H_9OH	360	474	2	455	19	471
8	C_6H_{12}	360	487	18	462	287	460
9	$C_6H_5CH_3$	360	490	2	486	33	465
10	CH_3COOCH_3	360	470	1.5	490	19	470
11	CH_3CN	360	484	1.4	500	15	476
12	CH_3CN + imidazole HCl	360	473	2	490	8	473

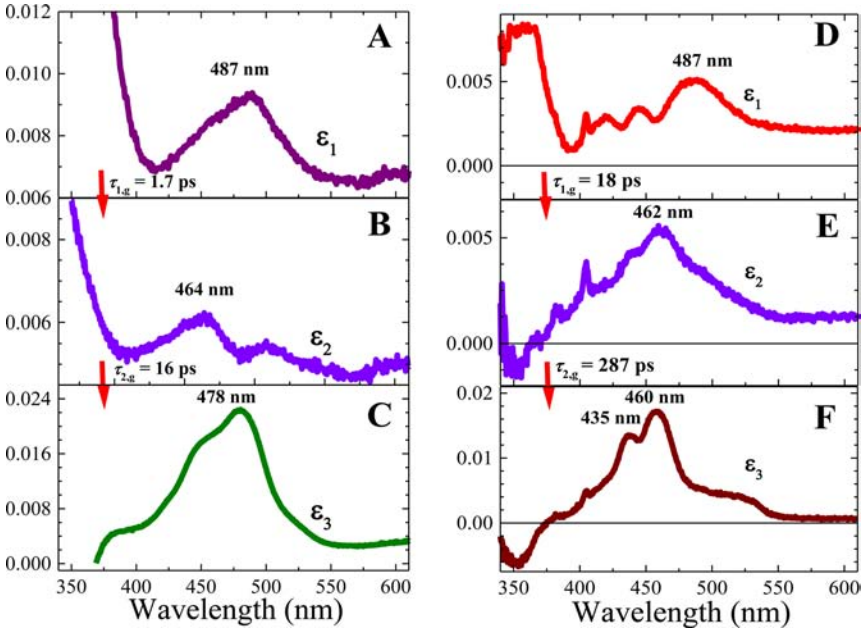

Figure 10. Decay-associated spectra (ε_i) and time constants ($\tau_{1,g}$ and $\tau_{2,g}$) extracted from the global fit of the ΔA spectra of **4** in 2-PrOH (A–C) and C_6H_{12} (D–F) upon 360-nm excitation.

Table 4. Quantum Yields of the Formation of the Triplet Nitrene 7 from 4 Excited at 350 nm

	solvent	$E_T(30)^f$	$\phi_{Tn}{}^a$	τ_2 (ps)^b	k_{ISC} (10^{10} s^{-1})^d	$\phi_p{}^c$	k_p (10^{10} s^{-1})^e
1	CH_3OH	55.4	0.30	10.5 ± 1.0	2.9	0.7	6.6
2	*n*-C_4H_9OH	49.7	0.68	17.5 ± 0.8	3.9	0.32	1.8
3	$(CH_3)_2CHOH$	48.4	0.84	16.5 ± 0.6	5.1	0.16	0.97
4	CH_3CN	45.6	1	8.1 ± 0.7	12.3	0	0
5	C_6H_{12}	30.9	1	280 ± 21	0.35	0	0

[a]Quantum yields for the formation of **7**. [b]Mean time constants averaged over the τ_2 entries in Tables 1–3S (Supporting Information) and Table 3. [c]Protonation quantum yields of the closed-shell nitrene **6**: $\phi_p = 1 - \phi_{Tn}$. [d]ISC rate constants: $k_{ISC} = \phi_{Tn}\tau_2$. [e]Protonation rate constants: $k_p = \phi_p\tau_2$. [f]Reference 43.

(Table 4). As a measure of strength of interaction of these species with the solvent, we used the $E_T(30)$ polarity parameter.[43] We assume that the visible ΔA amplitude quantifies the amount of **7** formed. This is justified as **5** has the red-shifted transitions of low oscillator strengths. The formation of **7** in C_6H_{12}, where no protonation is possible, has unit quantum yield ($\phi_{Tn,c} = 1$). Triplet–triplet absorption in C_6H_{12} is used for the determination of the quantum yield of the formation of the triplet species (ϕ_{Tn}) in other solvents using eq 1:

$$\frac{\alpha_{Tn}}{\alpha_{Tn,c}} \times \frac{\varepsilon_{Tn,c}}{\varepsilon_{Tn}} \times \varphi_{Tn,c} = \varphi_{Tn} \quad (1)$$

The α_{Tn} and $\alpha_{Tn,c}$ slopes of the dependence of the ΔA signal at the visible band maximum versus excitation energy were measured under the same experimental conditions at t = 100 ps (1000 ps in C_6H_{12}) when the band formation is complete. The maximum extinction coefficients of the visible band of **5** in C_6H_{12} ($\varepsilon_{Tn,c}$) and other solvent (ε_{Tn}) were evaluated on the basis of the conservation rule of the transition dipole moment strength (μ),[44] eq 2:

dx.doi.org/10.1021/ja405637b | J. Am. Chem. Soc. 2013, 135, 19167–19179

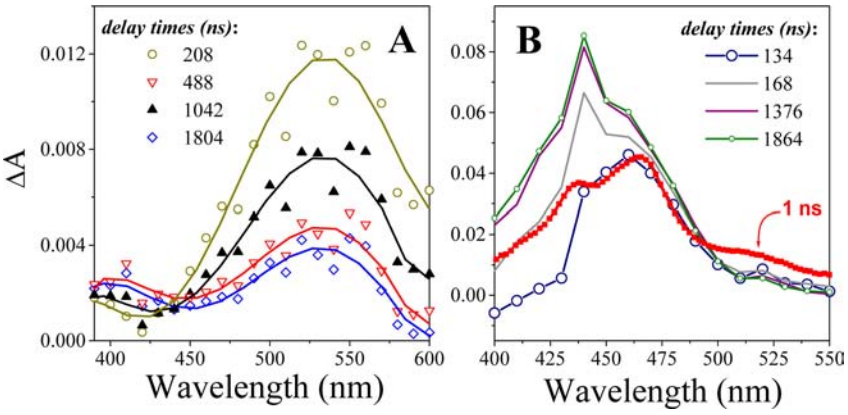

Figure 11. ΔA spectra of **4** in *n*-BuOH (A) and toluene (B) at several delay times (shown in the legends) after 355-nm nanosecond excitation. In panel B, the ΔA 1-ns spectrum measured in ultrafast experiments in toluene solutions is scaled to the 134-ns ΔA spectrum.

$$|\mu|^2 = \text{const}\, n\bar{\nu}^{-1}\varepsilon_{\text{Tn}} \int_{\text{band}} S_{\text{Tn}}(\nu)\, \text{d}\bar{\nu} \quad (2)$$

In eq 2, n is the solvent refractive index, $S(\nu)$ is the spectral profile of the visible band normalized to unity at the maximum and plotted against wavenumber ($\bar{\nu}$). The ε values and the α-ratio in cyclohexane and acetonitrile were similar, which suggests $\phi_{\text{Tn}} = 1$ in CH_3CN. In the protic solvents, $\phi_{\text{Tn}} \ll 1$ (Table 4), for which smaller α_{Tn} slopes (e.g., a factor of 4.4 in MeOH) is a main reason, despite an offset by ε values smaller by a factor of 1.33, as compared to C_6H_{12}. We note that the above treatment assumes that (i) **6** converts only to **7**, which is justified as it is the only relaxation path readily available to **6**; see Discussion for more details; and (ii) there is only one radiationless decay channel in electronically excited **4** leading to **6** in unit quantum yield. The barrierless nature of the S_2, S_3 states of **4** and the similarity in quantum yields for C_6H_{12} and CH_3CN solutions of drastically different polarity support the second assumption. We determined $\varepsilon_{\text{Tn}}(475\text{ nm}) = 5415\ M^{-1}\ cm^{-1}$ of **7** in CH_3CN using $\phi_{\text{Tn}} = 1$ and the benzophenone actinometer in benzene,[45−48] where the triplet state ($\varepsilon_{\text{Tb,max}}(532\text{ nm}) = 7220\ M^{-1}\ cm^{-1}$[46]) is formed in unit quantum yield ($\phi_{\text{Tb}} = 1$[45]). Then, quantum yields upon 255-nm excitation of **4** were measured using benzophenone in CH_3CN ($\phi_{\text{Tb}} = 1$,[45] $\varepsilon_{\text{Tb,max}}(525\text{ nm}) = 6250\ M^{-1}\ cm^{-1}$[46]). The values obtained were similar to those upon 350-nm excitation within the experimental uncertainty of 20%.

Microsecond Transient Absorption. Figure 11A shows the ΔA spectra of **4** in *n*-BuOH after excitation at 355 nm. A broad absorption band at 530−550 nm decays concurrently with a rise of the 380−410-nm absorption (time constant, 670 ns) . In 2-PrOH and *t*-BuOH, the ΔA spectra of **4** behave similarly, displaying a 2.5-μs decay time constant of the 530−550-nm band. Importantly, **4** in toluene (Figure 11B) gives rise to a much larger ΔA signal compared to *n*-BuOH under the same excitation conditions. In toluene, the 460-nm ΔA band (134 ns) greatly resembles the 1-ns ΔA spectrum in our ultrafast experiments. From 134 to 1864 ns, another absorption band at 440 nm develops.

DISCUSSION

Photochemical Reaction Paths. The 340- and 280-nm bands are assigned as $S_0 \rightarrow S_2$ and $S_0 \rightarrow S_3$, based on the agreement between their positions and relative intensities with the predictions from the CASPT2 calculations. The $S_0 \rightarrow S_1$ transition carries a negligibly small oscillator strength and, consequently, is absent in the spectrum. We conclude that the CASPT2 calculations accurately reproduce the transitions from the ground S_0 state to the first three excited singlet (S_1, S_2, and S_3) states. The 255-nm excitation used in this study promotes **4** to S_3. On the other hand, 360-nm excitation is at the low-energy wing of the $S_0 \rightarrow S_2$ transition and therefore should promote **4** to S_2 without vibrational energy excess. Excitation at 310 nm can be assigned to the $S_0 \rightarrow S_2$ transition populating vibrational excited S_2, with some contribution from the overlapping $S_0 \rightarrow S_3$ transition.

According to the MEP calculations, excitation of **4** to S_1 results in N_2 elimination with the formation of the open-shell singlet nitrene, **8** (Figure 2). However, photoexcitation to S_1 seems not to be possible because of low oscillator strength of the $S_0 \rightarrow S_1$ electronic transition. Following excitation to the S_2 and/or S_3 states, **4** relaxes barrierlessly through two CIs (S_3/S_2 and S_2/S_1) to form the closed-shell singlet nitrene **6** (Figure 3). Because the $S_0 \rightarrow S_2$ and $S_0 \rightarrow S_3$ electronic transitions carry all the oscillator strength and lead to the same product (**6**), the photochemistry of **4** is not excitation-wavelength-selective. The presence of the S_3/S_2 CI easily accessible from the Franck−Condon regions on the S_3 and S_2 potential energy surfaces explains the lack of any appreciable fluorescence of **4**. Moreover, stimulated emission of **4** was not observed upon either 255- or 360-nm excitation, consistent with the excited molecule reaching the S_3/S_2 CI very rapidly (≪150 fs). ISC may occur with $10^{11}\ s^{-1}$ rate constants in molecules containing heteroatoms.[27,49] There is no evidence that ISC in **4** takes place on a 100-fs time scale, as was previously reported in the S_1 state of 1-nitronaphthalene.[50] Therefore, we conclude that the radiationless relaxation of **4** proceeds through the manifold of singlet excited states.

The radiationless decay pathways of the closed-shell singlet nitrene **6** include internal conversion to the open-shell singlet nitrene **8** and ISC to the triplet nitrene **7** (Scheme 4). The former path is highly forbidden[51,52] because the change in orbital angular momentum is not balanced by a corresponding change in electron spin angular momentum, but ISC is allowed from **6** to **7** because the angular momentum associated with the electron spin flip is coupled with the angular momentum associated with the redistribution of electron density between orthogonal molecular orbitals.[53] Indeed, the most intense vertical electronic transitions of **7** and **6** correspond to $\pi \rightarrow \pi^*$ and $n \rightarrow \pi^*$, respectively (Figure 4; in **7**: orbital 5 (HOMO) → orbital 7; in **6**: orbital 1 → orbital 8). Consequently, the

dx.doi.org/10.1021/ja405637b | J. Am. Chem. Soc. 2013, 135, 19167−19179

Scheme 4

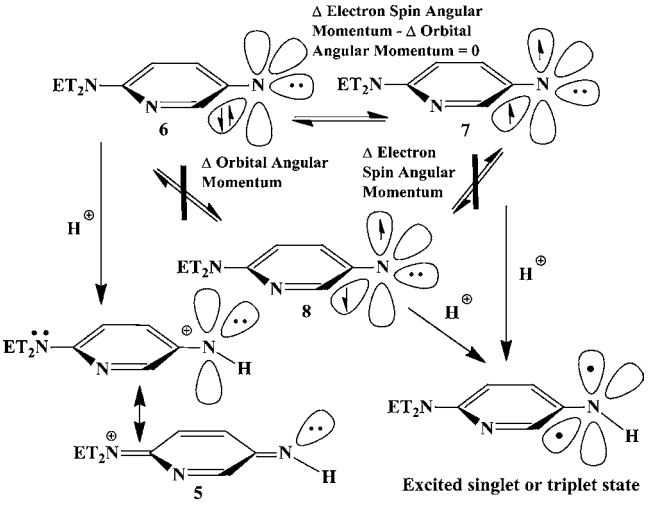

electronic configurations of **7** and **6** correspond to $^3(\pi, \pi^*)$ and $^1n^2$, respectively. Therefore, the only spin−orbit allowed processes are ISC back and forth between triplet and closed-shell singlet states.[53,54] For aromatic systems such as derivatives of aza-benzenes, -naphthalenes, and -phenanthrenes,[53,55] it is known that the fusion of N-heteroatoms into an aromatic ring significantly enhances ISC because of more efficient spin−orbit coupling between electronic configurations involving the nitrogen lone pair and π-orbitals. One would then expect fast ISC in **6** derived from **4**. Detailed studies of the photochemistry of the azide **1** reported the formation of a very basic closed-shell singlet nitrene that subsequently undergoes protonation in alcohol solvents on a several picoseconds time scale to yield a metastable nitrenium ion, in addition to undergoing less efficient ISC. The azide **4** investigated in this work is structurally related to **1**, and one might speculate that **6** may act as a proton acceptor in a manner analogous to that of the closed-shell singlet nitrene derived from **1** and that neither the open-shell singlet nitrene **8** nor the triplet nitrene **7** would be protonated since these attachments would lead to nitrenium ion excited states.

Ultrafast Dynamics. The S_2 and S_3 photochemical reactions of **4** are expected to proceed very rapidly (≪150 fs) as a result of the barrierless reaction paths and lead to elimination of N_2 with formation of the closed-shell nitrene **6**. Indeed, **6** (330−350 nm) was detected within the first 150 fs following excitation (Figure 6A). Numerous examples of intense UV (330−350 nm) absorption of singlet nitrenes derived from aryl azides are well-known.[14,56−58] Narrowing of the absorption of **6** and its time scale (τ_1), ranging from about 2 ps in polar solvents to 18 ps in cyclohexane, are typical of neutral polyatomic molecules as they dissipate their excess vibrationally energy to the surrounding solvent.[59−63] In cyclohexane, toluene, and methyl acetate, where protonation is not possible, **6** is expected to convert solely to **7** via ISC (time constant τ_2).

The visible transitions of **5** have low oscillator strengths in comparison to those of **7**, so that the absorption in the vicinity of the 450-nm band maxima is dominated by **7**. However, the visible ΔA absorption in protic and aprotic solvents of similar polarity (to minimize polarity effects on the band shape) is somewhat broader in the former solvents (Figure 9). This difference is observed as early as 20 ps after excitation (Supporting Information). This would be consistent with the formation of some nitrenium ions on a several picoseconds time scale. Furthermore, if **6** relaxes solely to **7**, the quantum yield for the formation of **7** should be unity in all solvents. However, the trend observed is that τ_2 becomes shorter but the triplet quantum yield decreases with the protic solvent polarity, suggesting the presence of competing reaction pathways, i.e., protonation and ISC. The τ_2 component is then due to both ISC and protonation in solvents where protonation is possible. The τ_2 values in 2-PrOH are independent of the photon energy (16.5 ps for 255-, 310- and 360-nm excitation, Table 4), suggesting that the ISC and protonation pathways originate from vibrationally relaxed **6**. The fact that **4** undergoes the consecutive photochemical reaction path with branching (ISC and protonation) occurring only during the last relaxation step allows one to interpret the transient cascade global fit as follows: ε_A is the hot **6** "instantaneously" formed upon excitation of **4**, ε_B is the cold **6** produced by relaxation of ε_A, and ε_C is the long-lived **7** or **7**/**5** generated as ε_B decays. For **6** that decays via two competing processes, ISC and protonation, its lifetime is $\tau_2 = 1/(\kappa_P + \kappa_{ISC})$, where κ_P is the protonation rate constant and κ_{ISC} is the ISC rate constant. The quantum yields for ISC (ϕ_{Tn}) and protonation (ϕ_P) are defined as: $\phi_{Tn} = \kappa_{ISC}\tau_2$ and $\phi_P = \kappa_P\tau_2$, with $\phi_P = 1 - \phi_{Tn}$, so that κ_{ISC} and κ_P can be determined. As shown in Table 4, κ_p increases with an increase of protic solvent polarity. These κ_p values are about three times smaller than those for the protonation reaction involving the closed-shell singlet nitrene species derived from the azide **1** in the same solvents.[14]

Nitrene Intersystem Crossing. Increasing polarity of the aprotic solvent leads to a dramatic acceleration of ISC in **6**: the κ_{ISC} increases by ∼34 times upon going from C_6H_{12} to CH_3CN (Figure 12 and Table 4). In the protic solvents, the trend is opposite: increasing polarity slows ISC with κ_{ISC} in MeOH smaller than that in 2-PrOH by a factor of ∼1.8. Seeking an explanation, we note that **6** has both nonbonding electrons localized on the same orbital of the N atom (the doubly occupied in-plane 2p-orbital (6), Figure 4), and as a result, its dipole moment is larger than that of the biradical triplet species.

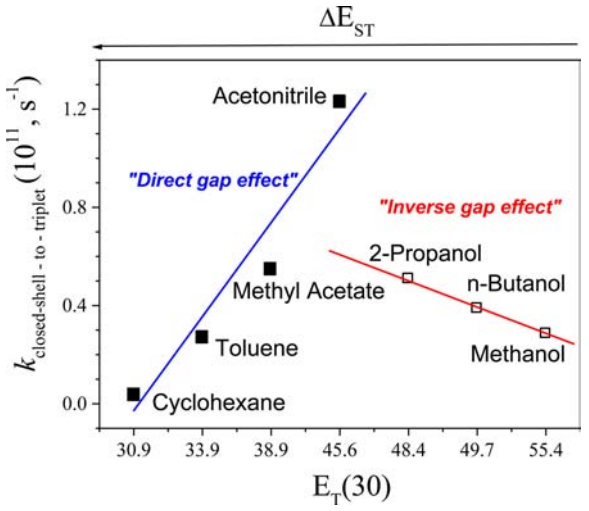

Figure 12. Intersystem crossing rate constants (κ_{ISC}) from the closed-shell singlet **6** nitrene to the triplet nitrene **7** as a function of a solvent polarity parameter $E_T(30)$. For cyclohexane, toluene, and methyl acetate, $\kappa_{ISC} = (\tau_2)^{-1}$. The κ_{ISC} entries for the remaining solvents are from Table 4.

dx.doi.org/10.1021/ja405637b | J. Am. Chem. Soc. 2013, 135, 19167−19179

As the solvent polarity increases, **6** is expected to be more strongly stabilized than **7**, which decreases the singlet−triplet energy gap between these two species. This conjecture is supported by the CASSCF(10,8)/6-31G* calculations of the energy gap between **6** and **7** (5.5 kcal mol^{-1} in MeOH vs 33 kcal mol^{-1} in vacuum).

With increasing singlet−triplet gap, ISC between the involved states generally decelerates. This is conventionally known as the "direct" energy gap law[23−25] and is explained by poorer Franck−Condon factors with increasing singlet−triplet energy gap.[23,24] The propensity rule indicates that the absorption of one quantum has the highest probability in the transition,[26] and as a result, the ISC transition probability is favored by high frequency vibrational modes (e.g., the C−H stretching vibrations).[25] Yet, ISC rate constants sometime increase with increasing energy gap. The so-called "inverse" gap effect[22] has been observed in aryl carbenes.[26] Usually, this is attributed to the lack of effective coupling between the singlet and triplet states separated by a small energy gap and having sparse manifolds of vibrational states. As the energy gap increases, the acceptor vibrational levels in the vicinity of the donor state become increasingly congested, leading to faster ISC. In words of Englman and Jortner, ISC from the closed-shell singlet **6** to triplet **7** nitrene is in the "weak coupling limit".[25] This case is observed in large molecules where the vibronic coupling is not very strong, giving rise to only slight displacements of the initial and final electronic potential energy surfaces. The **6** and **7** species indeed show very similar geometries with the modest maximum deviation in the bond lengths of ∼0.17 Å (Figure 5). The weak coupling limit predicts a large increase of ISC rate constants (roughly exponential for large gaps) with decreasing energy gap, which explains the large κ_{ISC} variation observed in the aprotic solvents. Polarity of protic solvents decreases the energy gap between **6** and **7**, and these species enter the small energy gap domain where the singlet−triplet gap becomes comparable to the frequency of the promoting high-frequency vibrational mode. With further increase of solvent polarity, the gap decreases further, and the promoter state density becomes sparse, weakening the coupling of vibronic states of **7** and **6** and causing slower ISC. This "inverse" gap law is observed from 2-PrOH to MeOH (Figure 12). In an alternative interpretation, the high-frequency mode may no longer be the coupling mode for small gaps, and lower-frequency promoting modes with weaker couplings may become more important.[22]

Protonation Mechanisms. On the basis of Figure 11B, the 460-nm ΔA band (134 ns) in toluene is assigned to **7**. This conclusion implies that in aprotic solvents, **7** is long-lived under our excitation conditions. In protic solvents, a much weaker ∼530-nm ΔA band (200 ns in *n*-BuOH, Figure 11A) may be explained by a relatively small extinction coefficient in the responsible species, such as the nitrenium ion **5**, Table 2. The 530-nm band is the precursor for the 410-nm absorption band, which on the basis of its spectral position (Table 2) can be attributed to the adduct **9** formed from the nitrenium ion **5**. A similar ΔA band following the decay of **7** is observed in methanol (Figure 8B, insert).

The photolysis of **4** in protic solvents leads to the formation of the addition products **10** in a very high yield (Table 1). It is clear that the precursor of the addition products **10** is the nitrenium ion **5**. In principle, this species can be formed by the protonation of either the closed-shell singlet or triplet nitrene.[64−66] The ΔA spectra of **4** reveal that a fraction of **6** undergoes protonation on a time scale of several tens of picoseconds, whereas the remaining fraction undergoes ISC to form **7**. However, since direct protonation of the triplet nitrene is less likely, since protonation of **7** to **5** requires a spin inversion.[67] Therefore, the most reasonable mechanism for the nitrenium ion formation is the protonation of the closed-shell singlet nitrene **6**. The next question we address is how to reconcile the observations of very high yields of both the addition products **10** (Table 1) and the triplet nitrene **7** (Table 4) in protic solvents.

A likely scenario is thermal activation of the triplet nitrene **7** coupled with reverse ISC into the closed-shell singlet nitrene **6**.[68−70] Such a mechanism has been invoked previously for protonation of the nitrene photochemically derived from 5-azido-8-methoxypsoralen.[70] Consequently, a closed-shell singlet nitrene reformed may reacts with a source of protons forming a nitrenium ion. Similar observations have been made previously by McClelland[70] and Bettinetti[68,69] and co-workers. Equilibrium was observed between singlet and triplet nitrenes derived from 5-azido-8-methoxypsoralen.[70] However, in this work the spin−orbital correlations between these species were not fully appreciated (Scheme 4), and the lower energy open-shell singlet nitrene was coupled with the triplet nitrene. In the present system, it has been shown that the closed-shell singlet nitrene is involved in this chemistry. With this adjustment, it now becomes clear how the nitrene might be stored in an unreactive triplet state and returned over relatively long periods of time via ISC to the reactive closed-shell singlet state, which is rapidly protonated to form the reactive nitrenium ion. However, such a situation is possible only if (i) in **6**, rate constants of protonation to **5** and direct ISC to **7** are comparable (Table 4); (ii) **6** and **7** are separated by a relatively small energy gap making the reverse ISC of **7** thermodynamically feasible at ambient temperatures (a 5×10^8 s^{-1} thermal activation rate constant for a 5.5 kcal mol^{-1} energy gap predicted by the Arrhenius expression[71] with a 5×10^{12} s^{-1} pre-exponential factor is consistent with a decay of **7** and a rise of **5** in methanol on a 2.5-ns time scale, Figure 8); and (iii) dimerization of **7** is much slower than reverse ISC of **7** and protonation of the reformed **6** (∼3% excited fraction of **4** (1.1 mM) upon our conditions suggests a 1 μs reaction time for dimerization of **6** with 10^{10} $M^{-1}s^{-1}$ second-order diffusion rate constants typical for the solvents investigated[72]). Therefore, the emerging picture is that a significant fraction of nascent **6** forms **7**. However, this triplet state is populated temporally, and **7** repopulates **6** on a time scale of several to several tens of nanoseconds determined by the solvent-dependent triplet-singlet energy gap. The reformed **6** subsequently undergoes rapid protonation. In a sense, this situation resembles the well-known, thermally activated delayed fluorescence phenomenon where the triplet excited state behaves as a "parking lot" for the fluorescing singlet excited state.[27] On the basis of the κ_P and κ_{ISC} rate constants (Table 4), we estimate that a fraction of **5** is formed directly on ultrafast time scales (e.g., about one-fifth in 2-PrOH), whereas the remaining fraction of **5** is formed more slowly as a result of thermally activated reverse ISC from **7** to **6** followed by protonation of **6**. As a result, the cross-linking product yield is 80−100% (Table 5).

Scheme 5 summarizes the reaction steps following photolysis of **4** in cyclohexane and 2-PrOH. In cyclohexane, a 287-ps lifetime of **6** is due to ISC to **7**, and **7** eventually forms the dimer **14** detected in product analysis (Scheme 3). The formation of the dimer **14** or aniline reduction product **12**

dx.doi.org/10.1021/ja405637b | J. Am. Chem. Soc. 2013, 135, 19167−19179

Table 5. Comparison of the Photochemical Characteristics of the Nitrophenyl Azide 1 and the New Azidopyridine 4

	1	4
addition products range, %	90−96	98−100
excitation wavelength, nm	305−420	260−350
irradiation time, h	4−6	2.5−4
conversion of starting material to products, %	50−70	100

Scheme 5

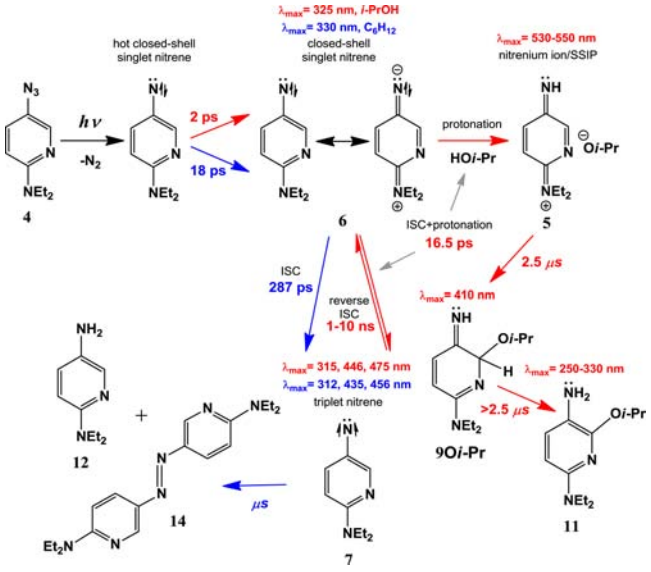

(possibly present in a microsecond time domain as a 440-nm absorption band, Figure 11B) is perfectly consistent with the formation of triplet nitrene in aprotic solvents. A 16.5-ps lifetime of **6** in 2-PrOH is due to ISC and protonation. A diiminoquinone-like species, the nitrenium ion **5**, stabilized by the electron-donating 4-amino group, slowly collapses forming the adduct **9**/cross-linked product **10**. We note that the protonation step should lead to the formation of a contact ion pair (CIP), which equilibrate to the solvent-separated ion pair (SSIP) via proton relay (Grotthuss mechanism[73−76]). The CIP to SSIP relaxation observed for **1** via some red shift in the CIP absorption band[14] is not detected in the present study for **4**, likely due to overlapping absorption of **7** and kinetic mechanisms involved in the formation of **5**.

CONCLUSIONS

The photochemical mechanism of 5-azido-2-(*N*,*N*-diethylamino)pyridine (**4**) in various solvents has been proposed on the basis of ultrafast and nanosecond transient absorption and product analysis, supported by multiconfigurational (CASSCF) and multireference (CASPT2) calculations. When **4** is excited to S_2 and S_3 states, it follows the ultrafast barrierless reaction path via two conical intersections toward the lowest singlet excited S_1 state, where N_2 elimination takes place. The nascent closed-shell singlet nitrene **6** is formed within the first 150 fs after excitation and undergoes vibrational relaxation with time constants ranging from 2 ps (polar solvents) to 18 ps (cyclohexane). In aprotic solvents, vibrationally relaxed **6** undergoes ISC on a solvent-dependent time scale of several to several hundred picoseconds, giving rise to the triplet nitrene **7**. The corresponding k_{ISC} rate constants increase and the energy gap between **6** and **7** decreases with increasing solvent polarity, and therefore these k_{ISC} values obey the "direct" gap law. In the protic solvents studied, vibrationally relaxed **6** undergoes both ISC to **7** and protonation to form the nitrenium ion **5**. An increase of the protic solvent polarity makes ISC slower, so these k_{ISC} values follow the "inverse" gap law. The protonation rate constants increase linearly with the increase in an empirical parameter of solvent polarity, $E_T(30)$. Experimental results suggest that ambient thermally activated reverse ISC of **7** to **6** in polar protic solvents is thermodynamically possible, which is supported by the CASSCF calculations of the energy gap between the closed shell singlet and triplet nitrenes in methanol (5.5 kcal mol^{-1}). As a result, **6** reformed from **7** tends to be protonated forming **5** within a time domain limited by the lifetime of **7**. In 2-PrOH, about four-fifths of the nitrenium ion **5** is produced via the aforementioned mechanism on a 10−100-ns time scale, whereas the remaining fraction is formed directly on an ultrafast time scale. In MeOH, this ratio is ∼50:50.

Product studies suggest that **4** is more efficient in the formation of cross-linked products compared to **1**. The first reason for the enhanced cross-linking efficiency is that the S_1 state of **1**, reached by excitation at 420 nm, is not reactive toward N_2 elimination: this S_1 excited state population returns back to the ground state. In **4**, the S_1 state is spectroscopically dark, and optical excitation can promote this system only to the higher-lying S_2 and S_3 excited states. The molecule then follows the barrierless ultrafast relaxation path to form the closed-shell singlet nitrene **6**. This species is a precursor to the nitrenium ion **5** and cross-linking product **10**. Thus, **1** can harvest only a part of the UV−vis spectrum for its cross-linking function, whereas the entire absorption spectrum of **4** is useful. The second reason is the relative energies of the closed-shell singlet and triplet nitrene species. In **4**, these species are separated by a relatively small energy gap, which is surmountable by thermal activation of the triplet molecules. As a result, the unreactive triplet state behaves as a "parking lot" for the highly reactive closed-shell singlet nitrene and the nitrenium ion. This process resembles the well-known phenomenon of thermally activated delayed fluorescence. In **1**, the energy gap between the triplet and the closed-shell singlet nitrenes is much larger and not surmountable via ambient thermal activation.

Consequently, the azide **4** offers substantial advantages over the azide **1** as a photoaffinity agent. Comparison of the photochemical characteristics of **1** with **4** is shown in Table 5. One of the main disadvantages of many aryl azides as PAL agents is their photoaffinity labeling at wavelengths shorter than 280 nm, the wavelengths of light leading to photochemical damage to the biological samples. The azide **4** is highly photoactive at wavelengths longer than 290 nm. Moreover, excitation of **4** leads to more efficient formation of cross-linked substitution products. It is noteworthy that even though **1** absorbs in the visible region, 420-nm excitation of **1** does not yield a nitrene. The coupling reactions of **4** proceed more efficiently than those of **1** with full conversion of starting material, and the photolysis of **4** in the presence of different nucleophiles form mainly addition products with fewer side products than **1**, which is probably due to the lack of unproductive nitro group photochemistry that occurs with **1**. Finally, the PAL conventional wisdom is that cross-linking should proceed rapidly following excitation of the PAL agent. While this happens to some degree with **4**, since a significant fraction of cross-linking does occur within a few picoseconds of excitation, a large portion the initially formed singlet nitrene is

dx.doi.org/10.1021/ja405637b | J. Am. Chem. Soc. 2013, 135, 19167−19179

converted into an unreactive triplet form that lives long enough to probe a variety of active sites or active site conformations. Furthermore, some of these sites will be more effective at initiating reverse ISC by virtue of their polarity or lack thereof. It shall be interesting to see how this type of site selectivity can affect PAL processes. Finally, the mechanism described here, equilibrium between closed-shell singlet and triplet nitrenes, finally accounts for the singlet-like reactivity that has been observed for triplet nitrenes in other systems.[68−70]

■ ASSOCIATED CONTENT

Supporting Information

Synthesis of starting material, product characterization, description of the time-resolved spectroscopic techniques used, CASCCF active-space orbitals of the azide **4** and nitrenes derived from **1** and **4**, minimum-energy CI Moplot topologies, optimized geometries and relative energies of the nitrenes, and transient absorption spectra of **4** in 2-PrOH upon 310-nm excitation and other solvents upon 360-nm excitation with full sets of the best-fit parameters. This material is available free of charge via the Internet at http://pubs.acs.org.

■ AUTHOR INFORMATION

Corresponding Author

rmw@bgsu.edu

Present Address

[†]Department of Chemistry, Emory University, Atlanta, GA 30322, United States.

Notes

The authors declare no competing financial interest.

■ ACKNOWLEDGMENTS

This work was supported by a NSF CAREER and MRI awards (Grants CHE-0847707 and CHE-0923360, A.N.T.) and the R. Marshall and Antonia G. Wilson Fund. An allocation of computer time from the Ohio Supercomputer Center is gratefully acknowledged.

■ REFERENCES

(1) Fleming, S. A. *Tetrahedron* **1995**, *51*, 12479−12520.
(2) Shehade, K. A. H.; Speilmann, H. P. *J. Org. Chem.* **2000**, *65*, 4949−4953.
(3) Dubinsky, L.; Krom, B. P.; Meijler, M. M. *Bioorg. Med. Chem.* **2012**, *20*, 554−570.
(4) Hashimoto, H.; Hatanaka, Y. *Eur. J. Org. Chem.* **2008**, 2513−2523.
(5) Robinette, D.; Neamati, N.; Tomer, K. B.; Borchers, C. H. *Expert Rev. Proteomics* **2006**, *3*, 399−408.
(6) Khodyreva, S. N.; Lavrik, O. I. *Curr. Med. Chem.* **2005**, *12*, 641−655.
(7) Hatanaka, Y.; Sadakane, Y. *Curr. Top. Med. Chem.* **2002**, *2*, 271−288.
(8) Wilson, R. M., Voskresenska, V. In *Nitrene and Nitrenium Ions (Wiley Series of Reactive Intermediates in Chemistry and Biology)*; Falvey, D., Ed.; Wiley: New York, 2013; pp 77−116.
(9) Escher, E. H. F.; Robert, H.; Guillemette, G. *Helv. Chim. Acta* **1979**, *62*, 1217−1222.
(10) Addo, J. K.; Swamy, N.; Ray, R. *Bioorg. Med. Chem. Lett.* **2002**, *12*, 279−281.
(11) Mauri, L.; Prioni, S.; Loberto, N.; Chigorno, V.; Prinetti, A.; Sonnino, S. *Glycoconjugate J.* **2003**, *20*, 11−23.
(12) Sedlák, E.; Panda, M.; Dale, M. P.; Weintraub, S. T.; Robinson, N. C. *Biochemistry* **2006**, *45*, 746−754.
(13) Lormann, M. E. P.; Walker, C. H.; Es-Sayed, M.; Braese, S. *Chem. Commun.* **2002**, *12*, 1296−1297.
(14) Voskresenska, V.; Wilson, R. M.; Panov, M.; Tarnovsky, A. N.; Krause, J. A.; Vyas, S.; Winter, A. H.; Hadad, C. M. *J. Am. Chem. Soc.* **2009**, *131*, 11535−11547.
(15) Peon, J.; Polshakov, D.; Kohler, B. *J. Am. Chem. Soc.* **2002**, *124*, 6428−6438.
(16) Pines, E.; Pines, D.; Barak, T.; Magnes, B. Z.; Tolbert, L. M.; Haubrich, J. E. *Ber. Bunsen-Ges. Phys. Chem.* **1998**, *102*, 511−517.
(17) Dias, M.; Mornet, R.; Laloue, M. *Bioorg. Med. Chem.* **1995**, *3*, 361−366.
(18) Dias, M.; Richomme, P.; Mornet, R. *J. Heterocycl. Chem.* **1996**, *33*, 1035−1039.
(19) De Waal, A.; Hartog, A. F.; de Jong, L. *Biochim. Biophys. Acta* **1987**, *912*, 151−155.
(20) Zhang, N.; Tomizawa, M.; Casida, J. E. *J. Med. Chem.* **2002**, *45*, 2832−2840.
(21) Sawanishi, H.; Tajima, K.; Tsuchiya, T. *Chem. Pharm. Bull.* **1987**, *35*, 4101−4109.
(22) Hollywood, F.; Nay, B.; Scriven, E. F.V.; Suschitzky, H.; Khan, Z. U. *J. Chem.Soc., Perkin Trans. 1* **1982**, 421−429.
(23) Schlag, E. W.; Schneider, S.; Fischer, S. F. *Annu. Rev. Phys. Chem.* **1971**, *22*, 465−526.
(24) Robinson, C. W.; Frosch, R. P. *J. Chem. Phys.* **1963**, *37*, 1962−1973.
(25) Robinson, C. W.; Frosch, R. P. *J. Chem. Phys.* **1963**, *38*, 1187−1203.
(26) Englman, R.; Jortner, J. *Mol. Phys.* **1970**, *18*, 145−164.
(27) Langan, J. G.; Sitzmann, E. V.; Eisenthal, K. B. *Chem. Phys. Lett.* **1984**, *110*, 521−527.
(28) Turro, N. J. *Modern Molecular Photochemistry*: University Science Books: Herndon, VA, 1991; p 147.
(29) Kovalenko, S. A.; Ernsting, N. P.; Ruthmann, J. *Chem. Phys. Lett.* **1996**, *258*, 445−454.
(30) Kovalenko, S. A.; Dobryakov, A. L.; Ruthmann, J.; Ernsting, N. P. *Phys. Rev. A* **1999**, *59*, 2369−2382.
(31) Rasmusson, M.; Tarnovsky, A. N.; Åkesson, E.; Sundstrom, V. *Chem. Phys. Lett.* **2001**, *335*, 201−208.
(32) Van Stokkum, I. H. M.; Larsen, D. S.; van Grondelle, R. *Biochim. Biophys. Acta, Bioenerg.* **2004**, *1657*, 82−104.
(33) Danilov, E. O.; Rachford, A. A.; Goeb, S.; Castellano, F. N. *J. Phys. Chem. A* **2009**, *113*, 5763−5768.
(34) Frisch, M. J. et al. In *Gaussian 03, revision C. 02*; Gaussian Inc.: Wallingford, CT, 2004.
(35) Aquilante, F.; De Vico, L.; Ferré, N.; Ghigo, G.; Malmqvist, P. Å.; Neogrády, P.; Pedersen, T. B.; Pitonak, M.; Reiher, M.; Roos, B. O.; Serrano-Andrés, L.; Urban, M.; Veryazov, V.; Lindh, R. *J. Comput. Chem.* **2010**, *31*, 224−247.
(36) Dunning, T. H., Jr. *J. Chem. Phys.* **1989**, *90*, 1007−1023.
(37) Houk, K. N. *J. Chem. Theory Comput.* **2005**, *1*, 70−77.
(38) Roos, B. O.; Taylor, P. R. *Chem. Phys.* **1980**, *48*, 157−173.
(39) Olkhov, R. V.; Matzinger, S.; Bally, T. *MoPlot (Molecular Orbital Plotting program)*, version 1.85 for Windows, Linux and MacOS X; University of Fribourg: Switzerland, 2005. See: http://www-chem-unifr.ch/tb/moplot/moplot.html.
(40) Schlegel, H. B. *J. Comput. Chem.* **2003**, *24*, 1514−1527.
(41) Andersson, K.; Malmqvist, P. A.; Roos, B. O. *J. Chem. Phys.* **1992**, *96*, 1218−1226.
(42) Olivucci, M. In *Computational Photochemistry*; Elsevier: Amsterdam, 2005; pp 92−128.
(43) Reinhardt, C. *Solvents and Solvent Effects in Organic Chemistry*; Wiley: New York, 2000; p 418.
(44) Mataga, N.; Kubota, T. *Molecular Interactions and Electronic Spectra*; Marcel Dekker: New York, 1970; chapter 3.
(45) Bensasson, R.; Gramain, J. C. *J. Chem. Soc., Faraday 1* **1980**, *76*, 1801−1810.
(46) Bonneau, R.; Carmichael, I.; Hug, G. L. *Pure Appl. Chem.* **1991**, *63*, 289−299.

(47) Hurley, J. K.; Sinai, N.; Linschitz, H. *Photochem. Photobiol.* **1983**, *38*, 9−14.
(48) El-Khoury, P. Z.; Tarnovsky, A. N. *Chem. Phys. Lett.* **2008**, *453*, 160−166.
(49) Shah, B. K.; Rodgers, M. A. J.; Neckers, D. C. *J. Phys. Chem. A* **2004**, *108*, 6087−6089.
(50) Zugazagoitia, J. S.; Almora-Díaz, C. X.; Peon, J. *J. Phys. Chem. A* **2008**, *112*, 358−365.
(51) Wang, J.; Kubicki, J.; Hilinski, E. F.; Mecklenburg, S. L.; Gustafson, T. L.; Platz, M. S. *J. Am. Chem. Soc.* **2007**, *129*, 13683−13690.
(52) Borden, W. T.; Gritsan, N. P.; Hadad, C. M.; Karney, W. L.; Kemnitz, C. R.; Platz, M. S. *Acc. Chem. Res.* **2000**, *33*, 765−771.
(53) Lower, S. K.; El-Sayed, M. A. *Chem. Rev.* **1966**, *66*, 199−241.
(54) Borden, W. T.; Gritsan, N. P.; Hadad, C. M.; Karney, W. L.; Kemnitz, C. R.; Platz, M. S. *Acc. Chem. Res.* **2000**, *33*, 765−771.
(55) Schmidt, K.; Brovelli, S.; Coropceanu, V.; Beljonne, D.; Cornil, J.; Bazzini, C.; Caronna, T.; Tubino, R.; Meinardi, F.; Shuai, Z.; Bredas, J. L. *J. Phys. Chem. A* **2007**, *111*, 10490−10499.
(56) Gritsan, N. P.; Platz, M. S. *Adv. Phys. Org. Chem.* **2001**, *36*, 255−304.
(57) Gritsan, N. P.; Platz, M. S. *Chem. Rev.* **2006**, *106*, 3844−3867.
(58) *Reactive Intermediate Chemistry*; Platz, M. S., Moss, R. A., Platz, W. S., Jones, M., Jr., Eds.; Wiley-Interscience: Hoboken, NJ, 2004; pp 501−560.
(59) Elsaesser, T.; Kaiser, W. *Annu. Rev. Phys. Chem.* **1991**, *42*, 83−107.
(60) Owrutsky, J. C.; Raftery, D.; Hochstrasser, R. M. *Annu. Rev. Phys. Chem.* **1994**, *45*, 519−555.
(61) Iwata, K.; Hamaguchi, H. *J. Phys. Chem. A* **1997**, *101*, 632−637.
(62) Baskin, J. S.; Yu, H.-Z.; Zewail, A. H. *J. Phys. Chem. A* **2002**, *106*, 9837−9844.
(63) Hamm, P.; Ohline, S. M.; Zinth, W. *J. Chem. Phys.* **1997**, *106*, 519−529.
(64) Chehade, K. A. H.; Speilmann, H. P. *J. Org. Chem.* **2000**, *65*, 4949−4953.
(65) Wang, J.; Kubicki, J.; Platz, M. S. *Org. Lett.* **2007**, *9*, 3973−3976.
(66) Anderson, G. B.; Falvey, D. E. *J. Am. Chem. Soc.* **1993**, *115*, 9870−9871.
(67) Srivastava, S.; Falvey, D. E. *J. Am. Chem. Soc.* **1995**, *117*, 10186−10193.
(68) Albini, A.; Bettinetti, G.; Minoli, G. *J. Am. Chem. Soc.* **1991**, *113*, 6928−6934.
(69) Albini, A.; Bettinetti, G.; Minoli, G. *J. Am. Chem. Soc.* **1999**, *121*, 3104−3113.
(70) Ramlall, P.; Li, Y.; McClelland, R. A. *J. Chem. Soc., Perkin Trans. 2* **1999**, 1601−1607.
(71) Scroeder, J.; Troe, J. In *Activated Barroer Crossing: Applications in Physics, Chemistry and Biology*; Hänggi, P., Fleming, G. R., Eds.; World Scientific: Simgapore, 1993; pp 206−240.
(72) Murov, S. L.; Carmichael, I.; Hug, G. L. *Handbook of Photochemistry*; Marcel Dekker: New York, 1993; p 207.
(73) Cukierman, S. *Biochim. Biophys. Acta* **2006**, *1757*, 876−885.
(74) Voth, G. A. *Acc. Chem. Res.* **2006**, *39*, 143−150.
(75) Markovitch, O.; Chen, H.; Izvekov, S.; Paesani, F.; Voth, G. A.; Agmon, N. *J. Phys. Chem. B* **2008**, *112*, 9456−9466.
(76) http://www.lsbu.ac.uk/water/grotthuss.html